A Comparison of Velocimetry Algorithms: Orthogonal Dynamic Programming Based Particle Image Velocimetry Versus Local Correlation Tracking

Tatsuya KOBAYASHI[1,2], Ryohtaroh T. ISHIKAWA[3,4], Motoki NAKATA[1,2], Takayoshi OBA[3] and Yukio KATSUKAWA[3]

[1]*National Institute for Fusion Science, National Institutes of Natural Sciences, Toki 509-5292, Japan*
[2]*The Graduate University for Advanced Studies, SOKENDAI, Toki 509-5292, Japan*
[3]*National Astronomical Observatory of Japan, Mitaka 181-8588, Japan*
[4]*Institute for Space-Earth Environmental Research, Nagoya University, Nagoya 464-8603, Japan*

(Received 1 May 2023 / Accepted 31 May 2023)

In the magnetic plasma fusion community and the solar physics research community, different velocimetry algorithms have been used. Those are: orthogonal dynamic programing based particle image velocimetry (ODP-PIV) and local correlation tracking (LCT), respectively. In this paper, a systematic comparison of these velocimetry codes is performed using synthetically produced turbulence data. The spatial scale of a typical turbulence pattern is scanned to examine the sensitivity of these codes on the tracer pattern property. Use of an LCT code is recommended when the ratio of the turbulence pattern size to the spatial resolution is small.

Keywords: plasma turbulence, magnetic fusion plasma, solar physics, velocimetry, orthogonal dynamic programming, local correlation tracking

DOI: 10.1585/pfr.18.1402058

1. Introduction

In magnetically confined plasmas, it is thought that turbulence driven transport primarily determines the plasma confinement properties. The amount of turbulent heat and particle transports greatly surpasses classical or neoclassical transport model prediction. Therefore, establishing a way to reduce the level of turbulent transport is mandatory for establishing an economically acceptable thermonuclear fusion plant. A potential approach for mitigating or even quenching the turbulent transport is to utilize cross-field plasma sheared flows [1], which are often generated spontaneously. The excitation mechanism of these flow structures are of significant interest for finding a control method over the turbulent transport, and therefore various approaches are underway [2].

In general, experimental determination of cross-field plasma flow is a great challenge. The $E \times B$ flow can directly be detected through plasma potential measurement by a multipoint heavy ion beam probe [3], although installation or operation of this dedicated diagnostic tool is allowed only in a limited situation. Spectroscopical methods, in which the Doppler shift of an emitted light spectrum line is analyzed to obtain the plasma flow velocity, are also feasible and applied in the L-H transition study [4, 5]. Spectroscopical techniques usually have a low time resolution and are not applicable to turbulence dynamics study. In addition, a cross-field line of sight needs to be set, which often requires in-vessel optics and dedicated heat shielding components [6].

Recently, significant progress has been made in development of two-dimensional fluctuation imaging diagnostics such as beam emission spectroscopy (BES) [7, 8] or electron cyclotron emission imaging (ECEI) [9]. By tracking the fluctuation pattern evolution in consecutive imaging frames, the plasma flow velocity field can be in principle estimated. This approach is in general called velocimetry. In the magnetic plasma fusion community, the so-called orthogonal dynamic programming (ODP) based particle image velocimetry (PIV) algorithm [10] is frequently used. This algorithm was originally developed in the neutral fluid physics community. By this method, a two-dimensional image is divided into multiple sub-stripes in vertical or horizontal directions. The fluctuation patterns are tracked one-dimensionally in consecutive time frames in each sub-stripe. The tracking is performed in the vertical and horizontal sub-stripes alternatively. Furthermore, the tracking is iteratively processed, in which the sub-stripe width is gradually narrowed. This iteration process helps to capture velocity field components with multiple spatial scales. ODP-PIV was applied in different experimental devices, and shed light on flow-turbulence interaction phenomena, such as geodesic acoustic mode dynamics [11], L-H transition mechanisms [12,13], and scrape off layer physics [14]. For those studies, various diagnostic systems were used, such as BES [11, 12], gas puff imag-

author's e-mail: kobayashi.tatsuya@nifs.ac.jp

ing (GPI) [13], and fast visible imaging [14]. Since this method is space domain-based and thus no time domain-based analysis is necessary, the velocity field can be evaluated at the time resolution of the data acquisition with no time-averaging.

Alternatively, a time domain-based cross-correlation technique, the so-called time-delay estimation (TDE), is also used for obtaining the two-dimensional velocity field [15]. Use of TDE is generally beneficial when the number of spatial points for measurement is limited. However, as TDE is a time domain-based method, the result is intrinsically time-averaged within a certain time period and suffers a deterioration in the time resolution [15]. In addition, unrealistically short time lag and high velocity are obtained when the turbulence packet propagates orthogonally across the row of the detector pair [16]. A comparison between TDE and ODP-PIV was given in [13].

In the solar physics research field, turbulent flows in the solar photosphere are considered to interact with magnetic fields and produce upward Poynting flux, which can lead to coronal heating, solar wind acceleration, and explosive phenomena [17, 18]. It is difficult to directly measure the flow velocity field in the orthogonal plane of the viewing line, while the velocity in the line-of-sight can be measured spectroscopically by the Doppler shift. Similar to the magnetic plasma fusion research field, the flow velocity field is often derived from two-dimensional imaging diagnostics. Evolution of convective turbulent patterns generated by typical cellular patterns on the solar photosphere, so-called granules, is tracked to obtain the pattern displacement that corresponds to the flow velocity. The algorithm conventionally used here is called local correlation tracking (LCT) [19]. LCT calculates the two-dimensional cross-correlation function between two consecutive images within a spatially localized weighting window. Analogous to ODP-PIV, the two-dimensional velocity field can be evaluated at the time resolution of the data acquisition when LCT is used. LCT directly quantifies two-dimensional correlation of images therefore is more intuitive than ODP-PIV, which alternatively performs vertical and horizontal one-dimensional cross-correlation analyses.

So far, these different space domain-based velocimetry algorithms have not been systematically compared, and therefore the relative merits and demerits of both have not been understood. In this paper, a systematic comparison of space domain-based velocimetry codes having different algorithms is performed, using synthetically produced turbulence data. The spatial scale of a typical turbulence pattern is scanned to examine the sensitivity of these codes on the tracer pattern property. Use of an LCT code is thought to be beneficial for fusion plasma diagnostic data where the ratio of the turbulence pattern size to the spatial resolution tends to be small.

2. Target Dataset

The dataset to be analyzed in the comparison is produced to be able to contrast the typical turbulent pattern size and the spatial resolution. In fusion research, ultrafast detectors such as an avalanche photodiode array are often used for imaging diagnostics, whose pixel number is often limited to, e.g., 8×8 pixels [8]. Therefore the ratio of the typical turbulence pattern size l_{corr} to the spatial resolution δ_{d} tends to be small, i.e., $l_{\mathrm{corr}}/\delta_{\mathrm{d}} < 5$. In other cases, a fast camera having larger pixel number, e.g., 64×80 pixels [15],

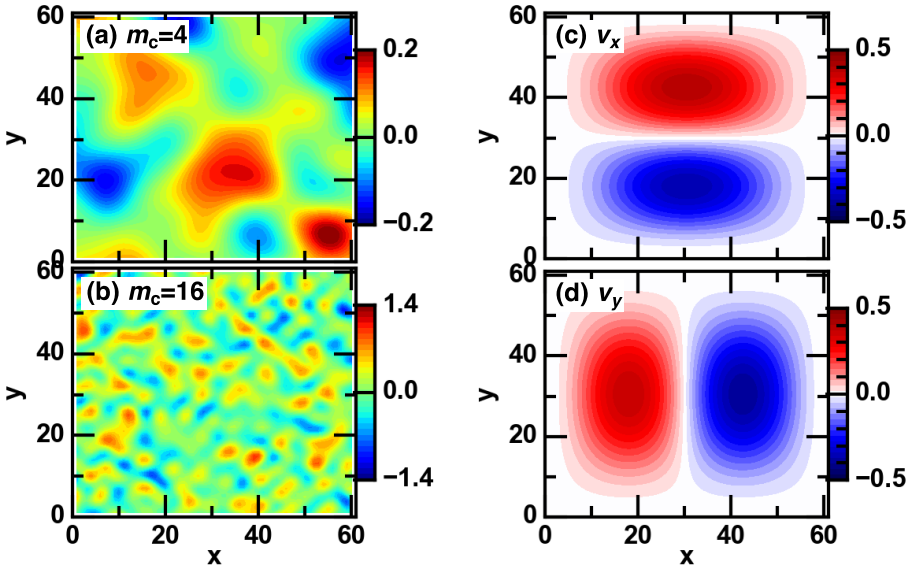

Fig. 1 Test turbulence pattern data generated with low-pass filters with cutoff modenumbers of (a) $m_{\mathrm{c}} = 4$ and (b) $m_{\mathrm{c}} = 16$, and test flow velocity in (c) x and (d) y directions.

is also used aiming for relatively slower target dynamics, in which the ratio $l_{\mathrm{corr}}/\delta_{\mathrm{d}}$ becomes larger. In the solar photosphere observation, a detector with a large pixel number is used, where the ratio $l_{\mathrm{corr}}/\delta_{\mathrm{d}}$ is typically larger than 50 for supergranulation and 5 to 10 for granulation [20]. By scanning the typical turbulence pattern size with a fixed set of the imaging span and resolution, the impact of the ratio of the turbulence pattern size to the spatial resolution on the velocimetry result is examined.

Test data are set on a 60×60 pixels in a two-dimensional plane. The turbulence pattern is generated from two-dimensional white Gaussian noise distribution by applying a spatial low-pass filter, both for x and y (horizontal and vertical) directions. The cutoff spatial scale $\lambda_{\mathrm{c}} = L/m_{\mathrm{c}}$ is defined, where $L = 60$ is the image span and $m_{\mathrm{c}} = 2(1 + j)$ with $j \in [1, 9]$ is the cutoff modenumber. Turbulence patterns generated with $m_{\mathrm{c}} = 4$ and $m_{\mathrm{c}} = 16$ are shown in Figs. 1 (a) and (b), respectively. Turbulence evolution is calculated by numerically solving the continuity equation with given velocity fields in the x and y directions as shown in Figs. 1 (c) and (d), respectively. This flow field corresponds to a clockwise rotation of the turbulence pattern, with zero velocity at the boundary. As it is not a rigid-body rotation, stretching of turbulence components can occur. Figure 2 shows the spatial modenumber spectrum in the x direction. An attempt to recover the given flow structure from the consecutive turbulence pattern images using different velocimetry algorithms is presented.

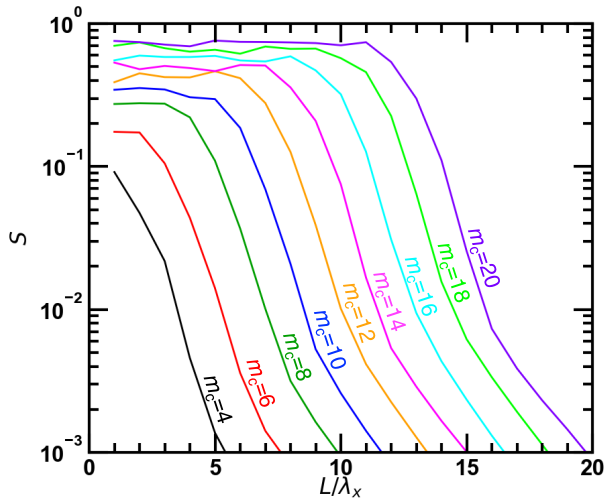

Fig. 2 Spatial modenumber spectrum of test turbulence patterns generated with different cutoff modenumbers m_{c}.

3. Results

As a practical LCT algorithm, two different codes are used here: Flowmaker [21, 22] and FLCT [23]. The former naively calculates the two-dimensional cross-correlation following the procedure in [19], while the latter performs this process in the Fourier domain. For both LCT and ODP-PIV algorithms, there is a similarly working smoothing kernel factor, FWHM. For LCT, the two-dimensional cross-correlation is calculated over the full area of the images, where localization is guaranteed by a Gaussian window function [19]. This Gaussian window function has the peak at the target pixel of analysis and has a factor FWHM that determines the spatial resolution. Therefore, local information with a certain spatial extent expressed by FWHM is effectively used for the velocity calculation. For ODP-PIV, the Gaussian filter having a spatial extent of the FWHM factor is applied at each iteration step, in order to smooth discontinuities among different sub-stripes.

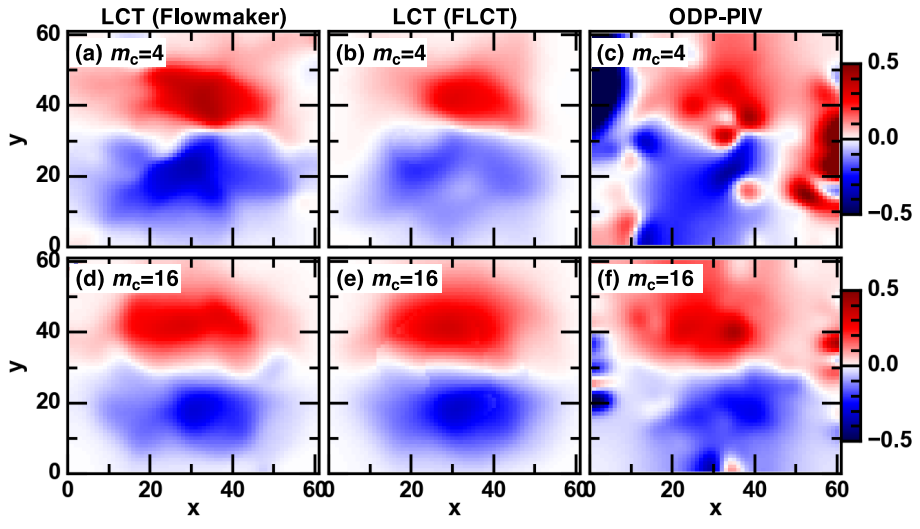

Fig. 3 Results of velocimetry in x direction obtained by (left) Flowmaker, (center) FLCT, and (right) ODP-PIV, for (top) $m_{\mathrm{c}} = 4$ and (bottom) $m_{\mathrm{c}} = 16$ turbulence pattern. Gaussian kernel FWHM factor of 8 is used.

For both cases, increasing FWHM improves the stability of the procedure, but degrades the spatial resolution. Figure 3 shows the results of velocimetry for the x coordinate velocity with FWHM = 8. Note that the y coordinate velocity estimation results are qualitatively similar to those of the x coordinate as shown in Fig. 4. In all cases, the given up-down inverse symmetric flow velocity field is recovered to a certain degree, although an artificial velocity fluctuation emerges. By comparing LCT and ODP-PIV, the former seems to give a better result. In ODP-PIV results, a large degree of error appears at the boundary. Both algorithms appear to work better when m_c is large. The systematic m_c dependence of estimation accuracy is given below. Figure 5 shows the results with FWHM = 20. Compared to the FWHM = 8 cases, the artificial velocity fluctuation becomes less prominent. Magnitude of the velocity is underestimated, particularly in the LCT results.

Estimation accuracy is examined by comparing the given v_x values to the estimated values. The comparisons are shown as joint probability density functions (PDFs) between $v_{x,\mathrm{given}}$ and v_x in Figs. 6 and 7 for FWHM = 8 and 20, respectively, and for different algorithms and m_c numbers. Dashed lines show $v_{x,\mathrm{given}} = v_x$. Features discussed above are confirmed: a better estimation by LCT, a small scatter of points with $m_c = 16$, and an estimate under of the magnitude of the velocity with FWHM = 20.

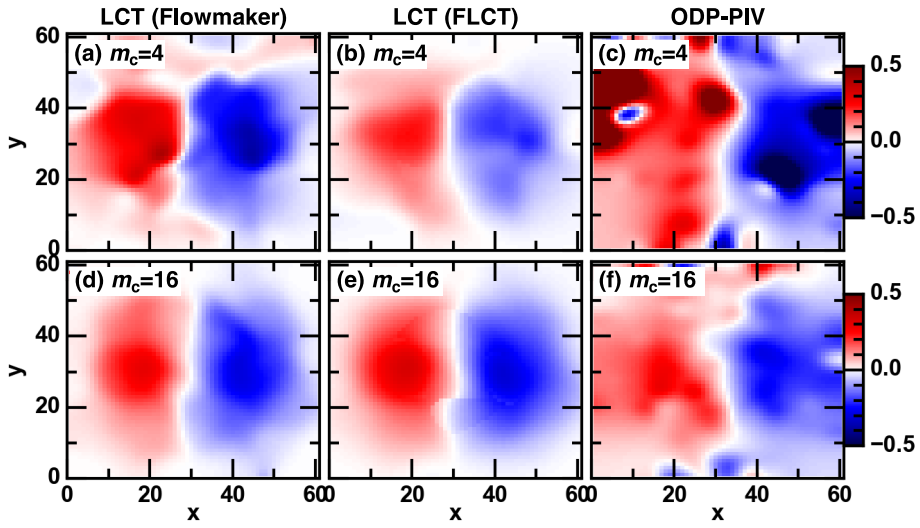

Fig. 4 Results of velocimetry in y direction obtained by (left) Flowmaker, (center) FLCT, and (right) ODP-PIV, for (top) $m_c = 4$ and (bottom) $m_c = 16$ turbulence pattern. Gaussian kernel FWHM factor of 8 is used.

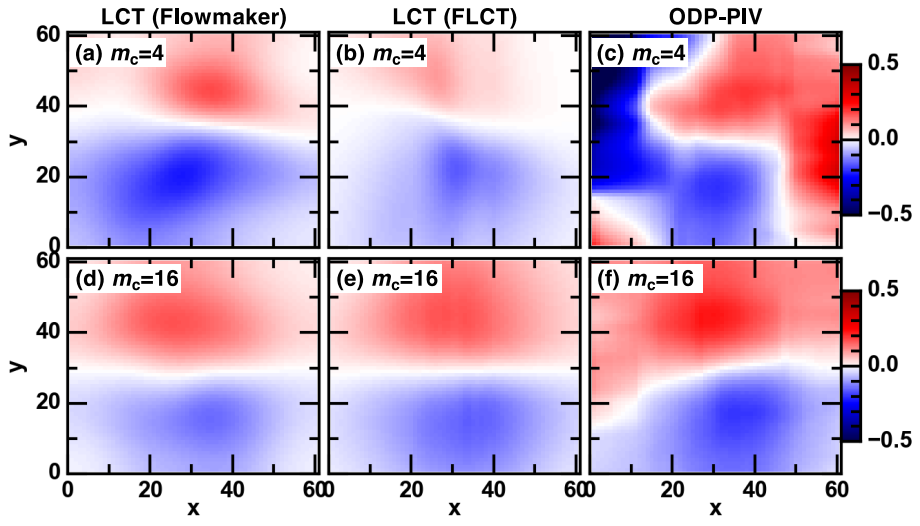

Fig. 5 Results of velocimetry in x direction obtained by (left) Flowmaker, (center) FLCT, and (right) ODP-PIV, for (top) $m_c = 4$ and (bottom) $m_c = 16$ turbulence pattern. Gaussian kernel FWHM factor of 20 is used.

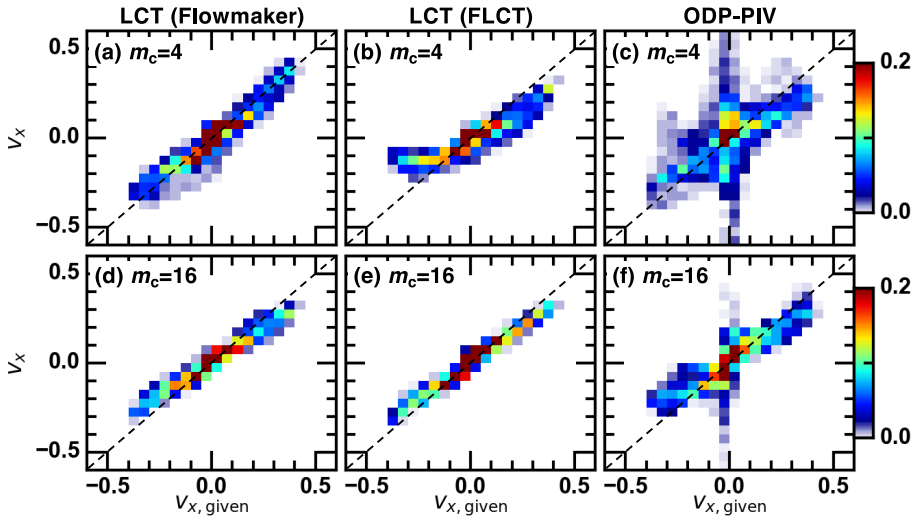

Fig. 6 Joint PDF between given x-velocity $v_{x,\mathrm{given}}$ and results of velocimetry v_x obtained by (left) Flowmaker, (center) FLCT, and (right) ODP-PIV, for (top) $m_c = 4$ and (bottom) $m_c = 16$ turbulence pattern. Gaussian kernel FWHM factor of 8 is used.

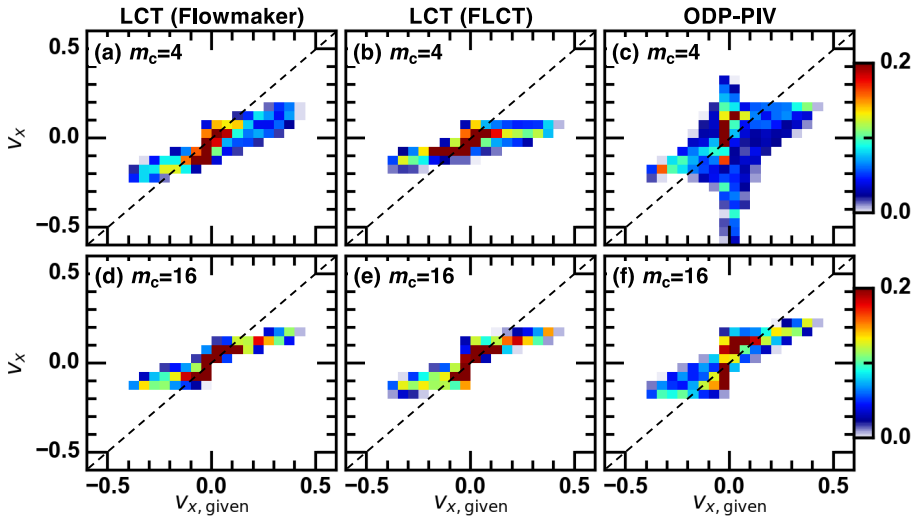

Fig. 7 Joint PDF between given x-velocity $v_{x,\mathrm{given}}$ and results of velocimetry v_x obtained by (left) Flowmaker, (center) FLCT, and (right) ODP-PIV, for (top) $m_c = 4$ and (bottom) $m_c = 16$ turbulence pattern. Gaussian kernel FWHM factor of 20 is used.

For a more quantitative comparison of different algorithms, m_c dependence of estimation accuracy is examined. Linear regression analysis between $v_{x,\mathrm{given}}$ and v_x is performed and the correlation coefficient and linear fitting slope are obtained as shown in Fig. 8. When the correlation coefficient is close to unity, the estimated result captures structural characteristics of the given flow velocity. The slope expresses the proportionality coefficient between $v_{x,\mathrm{given}}$ and v_x. When the slope is larger than unity, the velocimetry result underestimates the given velocity.

Looking at the Flowmaker results, the correlation coefficient saturates in $m_c \geq 8$, although it is reasonably high even in $m_c < 8$. Flowmaker tends to underestimate the flow velocity at a larger value of m_c. Estimation accuracy decreases when the value of FWHM is increased. The correlation coefficient for the FLCT results behaves similarly to that of the Flowmaker results, but the m_c dependence of the slope is opposite, i.e., an underestimation occurs when m_c is small. A better estimation with low FWHM value, similar to the Flowmaker case, is visible. While, in the ODP-PIV case, the correlation coefficient is notably small in $m_c < 8$, likely due to a boundary estimation error. If the same analysis is performed with data in $10 \leq x \leq 50$ and $10 \leq y \leq 50$, i.e., boundary data excluded, a significant improvement of the correlation coefficient is obtained. For example, in Figs. 6 (c) and (f), points with $v_{x,\mathrm{given}} \sim 0$ and finite values of v_x that come from boundary are excluded. The correlation coefficient at the condition of $m_c = 4$ and

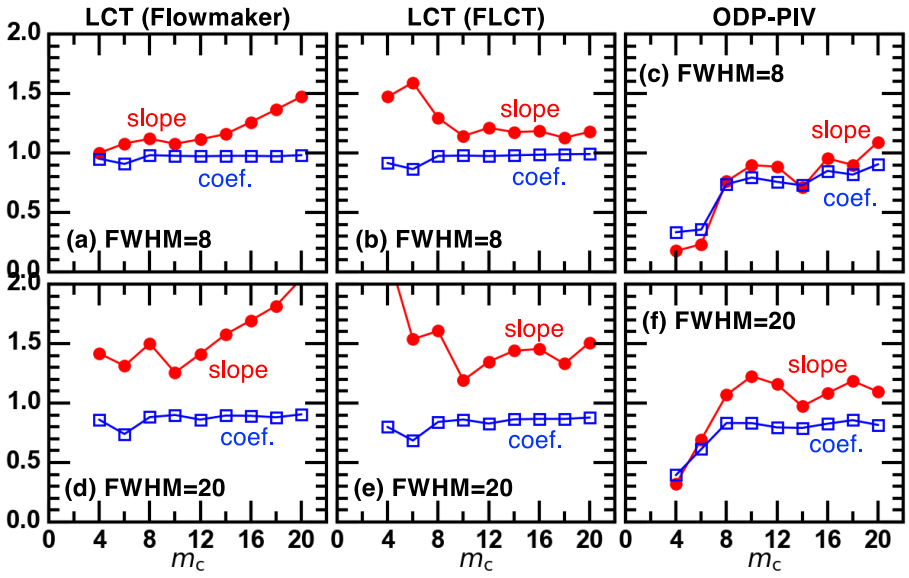

Fig. 8 Cutoff modenumber dependence of correlation coefficient and linear fitting slope between given velocity and results of velocimetry in x direction: (left) Flowmaker, (center) FLCT, and (right) ODP-PIV; and (top) FWHM = 8 and (bottom) FWHM = 20.

FWHM = 8 increases from 0.334 to 0.814. Increasing m_c improves the estimation accuracy to some extent. An underestimate of the flow velocity magnitude at larger m_c values is rather milder than in the LCT cases.

For practical use in analyzing fusion plasma diagnostic data, LCT-Flowmaker is expected to have advantages when m_c is small. A trial use of LCT-Flowmaker with fusion plasma data will be performed in future. In addition, a deep learning based velocity field estimation technique has recently been developed [24]. An application of this approach to magnetic plasma fusion data is also underway.

4. Summary

In this paper, a systematic comparison of different velocimetry codes was performed using synthetically produced turbulence data. The spatial scale of the typical turbulence pattern was scanned to examine the sensitivity of these codes on the tracer pattern property. Orthogonal dynamic programming based particle image velocimetry (ODP-PIV), which has been conventionally used in the magnetic plasma fusion community, was found to give inaccurate velocity fields at the image boundary. While, the local correlation tracking (LCT) code did not give such artifacts at the boundary, even with a larger turbulence pattern. Use of an LCT code was recommended when the ratio of the turbulence pattern size to the spatial resolution was small.

Acknowledgments

We thank M. Sasaki for a useful discussion. This study is supported by the NINS program for cross-disciplinary study on Turbulence, Transport, and Heating Dynamics in Laboratory and Astrophysical Plasmas: "SoLaBo-X" (Grant Numbers 01321802 and 01311904), by the NAOJ Research Coordination Committee, NINS (NAOJ-RCC-2201-0402 and -0403), and by the Grant-in-Aid for Scientific Research of JSPS (JP21K13902). RTI, TO, and YK acknowledge the financial support by the Grant-in-Aid for Scientific Research of JSPS (JP18H05234).

[1] H. Biglari, P.H. Diamond and P.W. Terry, Phys. Fluids B **2**, 1 (1990).
[2] T. Kobayashi, Nucl. Fusion **60**, 095001 (2020).
[3] T. Ido, Y. Hamada, A. Nishizawa, Y. Kawasumi, Y. Miura and K. Kamiya, Rev. Sci. Instrum. **70**, 955 (1999).
[4] R.J. Groebner, K.H. Burrell and R.P. Seraydarian, Phys. Rev. Lett. **64**, 3015 (1990).
[5] K. Ida, S. Hidekuma, Y. Miura, T. Fujita, M. Mori, K. Hoshino, N. Suzuki, T. Yamauchi, JFT-2M group *et al.*, Phys. Rev. Lett. **65**, 1364 (1990).
[6] M. Yoshinuma, K. Ida, M. Yokoyama, M. Osakabe and K. Nagaoka, Fusion Sci. Technol. **58**, 375 (2010).
[7] G.R. McKee, R.J. Fonck, D.K. Gupta, D.J. Schlossberg, M.W. Shafer, C. Holland and G. Tynan, Rev. Sci. Instrum. **75**, 3490 (2004).
[8] T. Kobayashi, M. Yoshinuma and K. Ida, Plasma Phys. Control. Fusion **62**, 125011 (2020).
[9] H. Park, E. Mazzucato, T. Munsat, C.W. Domier, M. Johnson, N.C. Luhmann Jr, J. Wang, Z. Xia, I.G.J. Classen, A.J.H Donné *et al.*, Rev. Sci. Instrum. **75**(10), 3787 (2004).
[10] G.M. Quénot, J. Pakleza and T.A. Kowalewski, Exp. Fluids **25**, 177 (1998).
[11] D.K. Gupta, G.R. McKee and R.J. Fonck, Rev. Sci. Instrum. **81**, 013501 (2010).
[12] Z. Yan, G.R. McKee, R. Fonck, P. Gohil, R.J. Groebner and T.H. Osborne, Phys. Rev. Lett. **112**, 125002 (2014).
[13] A. Diallo, S. Banerjee, S.J. Zweben and T. Stoltzfus-Dueck, Nucl. Fusion **57**, 066050 (2017).
[14] S. Banerjee, H. Zushi, N. Nishino, K. Mishra, T. Onchi, A.

Kuzmin, Y. Nagashima, K. Hanada, K. Nakamura, H. Idei *et al.*, Rev. Sci. Instrum. **86**, 033505 (2015).
[15] S.J. Zweben, A. Diallo, M. Lampert, T. Stoltzfus-Dueck and S. Banerjee, Phys. Plasmas **28**, 032304 (2021).
[16] T. Kobayashi, G. Birkenmeier, E. Wolfrum, F.M. Laggner, M. Willensdorfer, U. Stroth, S. Inagaki, S.-I. Itoh and K. Itoh, Rev. Sci. Instrum. **85**, 083507 (2014).
[17] S. Toriumi and H. Wang, Living Rev. Sol. Phys. **16**, 3 (2019).
[18] S.R. Cranmer and A.R. Winebarger, Annu. Rev. Astron. Astrophys. **57**, 157 (2019).
[19] L.J. November and G.W. Simon, Astrophys. J. **333**, 427 (1998).
[20] M. Rieutord and F. Rincon, Living Rev. Sol. Phys. **7**, 1 (2010).
[21] T. Darvann, Master's thesis, University of Oslo, 1991.
[22] R. Molowny-Horas and Z. Yi, ITA (Oslo) Int. Rep. page 31 (1994).
[23] G.H. Fisher and B.T. Welsch, *FLCT: a fast, efficient method for performing local correlation tracking*, In *Subsurface and atmospheric influences on solar activity*, vol. 383, p. 373 (2008).
[24] R.T. Ishikawa, M. Nakata, Y. Katsukawa, Y. Masada and T.L. Riethmüller, Astron. Astrophys. **658**, A142 (2022).